

# 1 Shake table tests on standard and innovative temporary partition walls

2 Crescenzo Petrone<sup>a</sup>, Gennaro Magliulo<sup>b</sup>, Gaetano Manfredi<sup>c</sup>

3 <sup>a</sup>University College London, Department of Civil, Environmental & Geomatic Engineering, Chadwick Building, WC1E 6BT London, UK

4 [c.petrone@ucl.ac.uk](mailto:c.petrone@ucl.ac.uk)

5 <sup>b</sup>University of Naples Federico II, Department of Structures for Engineering and Architecture, via Claudio 21, 80125 Naples, Italy,

6 [gmagliu@unina.it](mailto:gmagliu@unina.it)

7 <sup>c</sup>University of Naples Federico II, Department of Structures for Engineering and Architecture, via Claudio 21, 80125 Naples, Italy,

8 [gamanfre@unina.it](mailto:gamanfre@unina.it)

## 9 ABSTRACT

10 Shake table tests are performed on temporary internal partitions for office buildings. Four different  
11 specimens are tested. A steel frame is designed to exhibit relative displacements, which typically  
12 occur at a given story of ordinary buildings. Four different partition walls are tested simultaneously  
13 for each specimen typology. This allows investigating the influence of an innovative device on the  
14 seismic performance of the tested components. The innovative device aims at avoiding the  
15 unhooking of the panels from the supporting studs. Several shake table tests are performed  
16 subjecting the specimens to interstory drift ratios up to 1.57%. Both the hysteretic curves and the  
17 natural frequency trend highlight that the partitions do not contribute to the lateral stiffness of the  
18 test setup. The damping ratio increase after the partition walls are installed within the test frame,  
19 causing a beneficial effect in the dynamic response. Minor damage state occurs for interstory drift  
20 ratio (IDR) in the range 0.41-0.65 in standard specimens, whereas moderate and major damage  
21 states are attained for IDR in the range 0.51-0.95. Significant increase of collapse IDR is recorded  
22 with the introduction of the innovative device, up to IDR larger than 1.45%. It can be therefore  
23 concluded that a simple innovative device is defined, which significantly improves the seismic  
24 performance of the tested specimen.

25  
26  
27 *Keywords: nonstructural components, shake table, experimental tests, seismic fragility, dynamic*  
28 *identification*

## 31 1 INTRODUCTION

32 Several recent earthquakes highlighted the huge impact of nonstructural components on earthquake  
33 loss [1]. 2010 Darfield earthquake in New Zealand underlined that even in buildings with low  
34 damage to their structural systems, nonstructural and content damages can be significant [2]. Past  
35 earthquake reconnaissance reports underlined the enormous contribution of nonstructural  
36 components to the three Ds:

- 37 • Dollars: Most of the construction cost of a building is related to nonstructural components,  
38 up to 92% of the total cost for hospitals [3]. The loss related to the failure of nonstructural  
39 components may easily exceed the total cost of the building, if breakdown and loss of  
40 inventory are considered [4].
- 41 • Downtime: Nonstructural components generally exhibit damage for low seismic demand  
42 levels, which do not cause serious structural damage. The seismic performance of  
43 nonstructural components is especially important in frequent, i.e. less intense, earthquakes,  
44 in which their damage can cause the inoperability of structurally undamaged buildings.
- 45 • Deaths: nonstructural component damage can also threaten the life safety. Their damage  
46 may cause the obstruction of the ways in and/or out of buildings, which can cause human  
47 suffocation. In this sense, it should be noted that 64% of the fatalities caused by 1995 Great  
48 Hanshin Earthquake was due to the people suffocation [5].

49 This paper deals with temporary internal partitions which can be classified as architectural  
50 nonstructural components, according to Villaverde [6]. The attention of the research community has  
51 moved towards the seismic assessment of nonstructural components over the last decade. Several  
52 research studies can be found in the literature concerning the seismic assessment of nonstructural

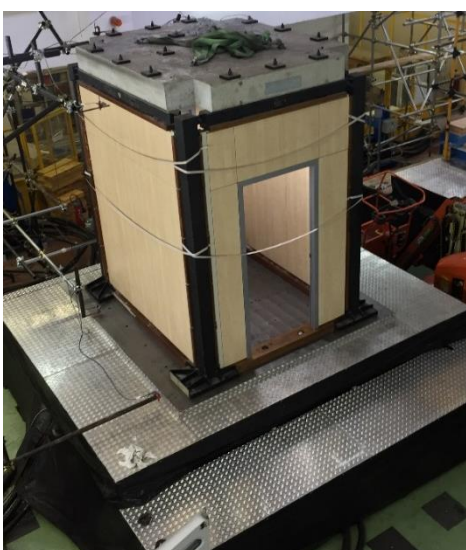
53 components, e.g. [7-14] among many others; many research activities focused on the experimental  
54 assessment for the seismic performance of components; some numerical studies were also  
55 developed based on such experimental campaigns.

56 Some studies dealt with the assessment of the performance of lightweight partition systems (and  
57 light office furniture) [15-17]. Extensive experimental campaigns were conducted at the State  
58 University of New York at Buffalo and at the University of Nevada [11, 18] However, the lack of  
59 previous studies on the seismic performance of temporary (mobile) internal partitions is clearly  
60 denoted in literature. This partition typology is worldwide spread particularly in office buildings.  
61 Some applications can be found also in airports, hospitals and commercial centers. Their seismic  
62 performance assumes a key role in the earthquake expected annual loss of these buildings, which  
63 are characterized by a large cost due to their evacuation. Finally, it should be underlined that these  
64 partitions are characterized by a peculiar construction technique; hence, they cannot be studied as  
65 other partition typologies.

66 Based on the above mentioned motivations, a shake table test campaign is conducted on temporary  
67 internal partitions. Four different specimens representative of typical European partitions are  
68 selected. These specimens are subjected to both in-plane interstory drifts and out-of-plane  
69 accelerations. An innovative device is also defined in order to improve the seismic performance of  
70 the partitions. Innovative and standard specimens are simultaneously tested in order to allow a  
71 direct comparison between their performances. The experimental setup, the input definition and the  
72 instrumentation are discussed in the following section. Then, the results of the shake table tests are  
73 summarized, focusing on typical damage typologies. Different damage states are correlated to an  
74 engineering demand parameter, highlighting the influence of the innovative device on the seismic  
75 behavior of the tested components.

## 76 **2 EXPERIMENTAL FACILITIES, TEST SETUP, SPECIMENS AND TESTING 77 PROTOCOL**

78 The shake table tests are carried out at the laboratory of the Department of Structures for  
79 Engineering and Architecture of the University of Naples Federico II in order to investigate the  
80 seismic behavior of temporary internal partitions. The test setup (Figure 1) is composed of (a) a  
81 shaking table simulator, (b) a 3D steel test frame (c) four partitions, one for each bay of the test  
82 frame. A 3 m × 3 m shaking table is used, which is characterized by two degrees of freedom in the  
83 two horizontal directions. The maximum payload is 200 kN with a frequency range of 0-50 Hz,  
84 peak acceleration, associated to the maximum payload, equal to 1.0g, peak velocity equal to 1 m/s  
85 and total displacement equal to 500 mm ( $\pm 250$  mm). Test setup properties, specimens, shake table  
86 input and instrumentation are discussed in the following paragraphs.



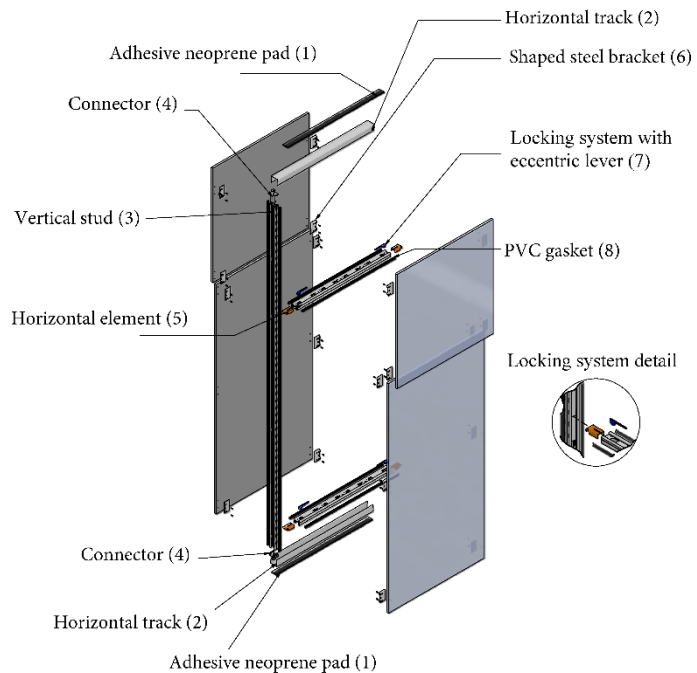
88  
89 **Figure 1. Global view of the test setup**

90    **2.1 Test setup and specimens**

91    The test frame is designed in order to dynamically excite the specimen, subjecting it simultaneously  
92    to in-plane interstory drifts and out-of-plane accelerations. It is designed to exhibit relative  
93    displacements which typically occur at a given story of ordinary buildings. In fact, it has been  
94    equipped with a realistic mass, i.e. mass per unit area equal to  $1.0 \text{ t/m}^2$ , and a lateral stiffness typical  
95    of ordinary buildings; the interstory displacement is assumed to be equal to 0.005 times the  
96    interstory height, for a “frequent” (i.e. 50 years return period) earthquake typical of high seismicity  
97    areas. Indeed, the test frame is designed in order to exhibit a 0.5% interstory drift for an earthquake  
98    characterized by  $S_{\text{DS},50}$  equal to 0.60 g. Such an intensity level is representative of an earthquake  
99    with 0.24 g peak ground acceleration, i.e. an intensity level of earthquake with 50 years return  
100   period in a high seismicity zone according to the indications included in [19]. A parametric study is  
101   required in order to accomplish the different requirements, as detailed in [9]. The definition of the  
102   test response spectrum (see section 2.2) ideally ensures that the accelerations acting on the  
103   component are realistic for the chosen intensity level. For instance, when interstory drift reaches  
104   0.5%, the acceleration on flexible components equals 1.6 times  $S_{\text{DS},50}$ , i.e. 0.96g. The design natural  
105   frequency of the test setup is equal to 4.17 Hz. It should be acknowledged that the frequency of the  
106   setup certainly affects the number of cycles subjected to the specimen. Moreover, the use of a single  
107   story test setup certainly causes large acceleration amplification from the base to the top of the test  
108   frame, which is larger than in two adjacent floors in a high-rise building.

109   The shake table tests aim at investigating the seismic performance of temporary partitions. Four test  
110   campaigns are executed on four different partition typologies. The partitions are characterized by an  
111   internal steel structure which is externally covered by wood, glass or steel panels. In particular, the  
112   different components are installed in the following order (Figure 2).

- 5 mm thick bi-adhesive neoprene pads are bonded at the base and at the top of the partition, (1) in Figure 2.
- Two horizontal U-section tracks at the base and the top are bonded to the bi-adhesive neoprene pads, (2) in Figure 2.
- Two vertical U-section tracks, one on the right and one on the left, are connected to wooden elements.
- Vertical studs, consisting of C-shaped cold-formed steel elements, (3) in Figure 2, are housed in the horizontal tracks. The studs are in contact with the tracks by means of special devices, (4) in Figure 2; these devices (Figure 3) are activated through a screwdriver, which induces a compressive force in the studs and a consequent friction resistance at the stud-to-track connection. The connection of the studs with the tracks is therefore based on friction. Moreover, several slotted holes are provided along the vertical studs to allow the hooking of the panels.
- A steel compensation profile is housed in one of the two vertical guides and is rigidly connected to a steel stud (Figure 4).
- Horizontal elements, (5) in Figure 2, consisting of C-shaped cold-formed steel elements, connect two adjacent vertical studs. The horizontal elements can be connected to the studs either via screws or through a locking system, (7) in Figure 2, consisting of an eccentric lever.
- Panels, made with different materials, are hooked into the slotted holes in vertical studs. Panels have suitably shaped edges to permit such a connection with the exception of wooden panels (Figure 5). For wooden panels, properly shaped steel brackets are adopted, (6) in Figure 2. The gap among adjacent panels is limited to 4 mm for aesthetic reasons. Panels are typically hooked into studs except the lateral panels which are not connected to the compensation profile; these panels are linked with spring constraints to the lateral guide (Figure 6). PVC gaskets, (8) in Figure 2, are positioned on the studs and on the horizontal elements, in order to improve the acoustic performance of the partition.



140

141

**Figure 2. Exploded view of temporary partitions with wood panels**



**Figure 3. Connector devices used in the partitions**

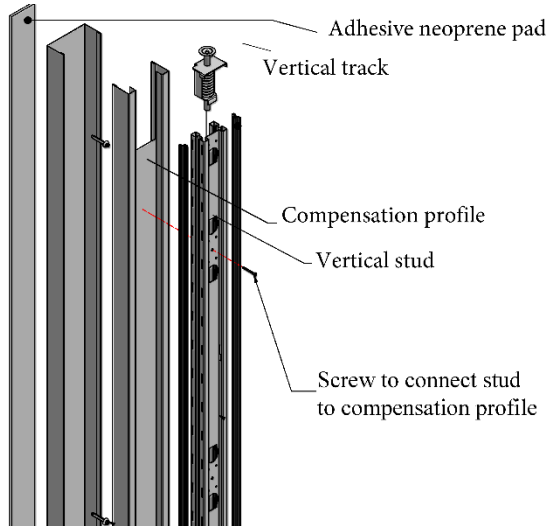
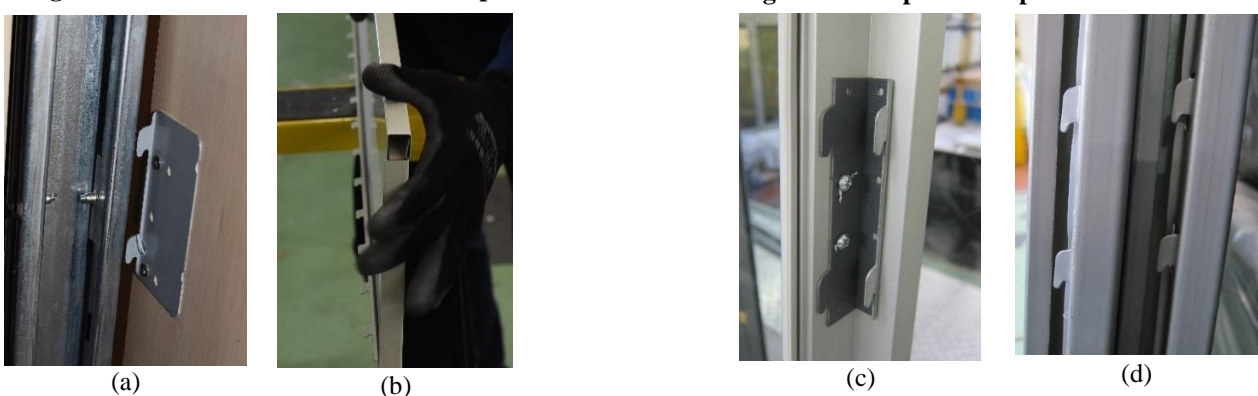


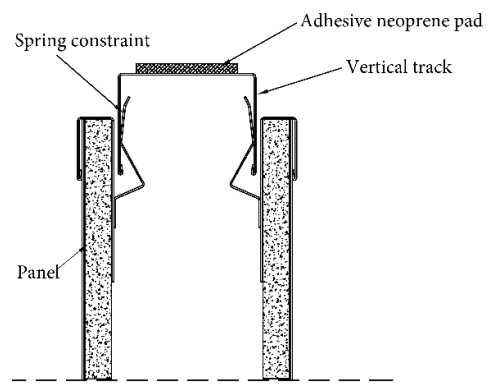
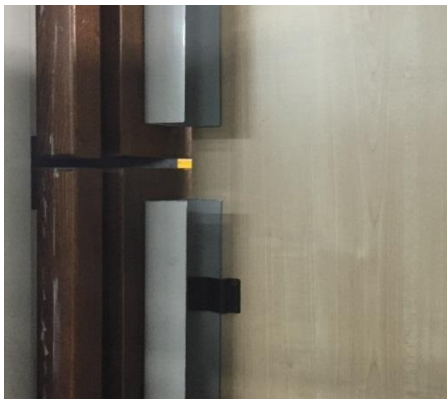
**Figure 4. Compensation profile**



142

143

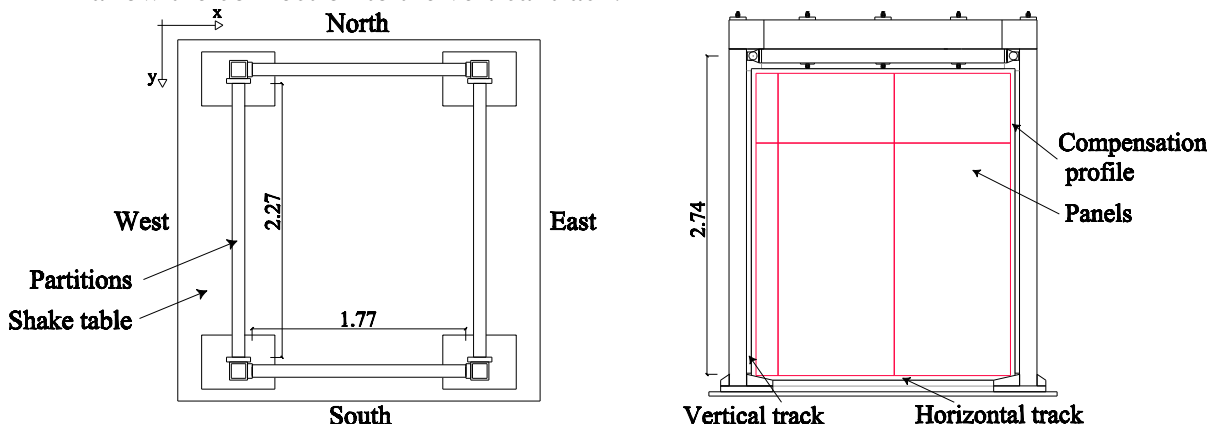
**Figure 5. Panel hooking systems: a) wood panels; b) steel panels; c) glass panels with aluminum frame; d) glass panels with steel frame**



144  
145 **Figure 6. Connection between lateral track and panel through spring constraint**

146 For each specimen, four partitions are simultaneously tested in order to maintain symmetry of the  
147 test frame. The plan and lateral view of the tested specimens and the walls ID are shown in Figure  
148 7. Four different partition typologies are tested (Figure 8):

- 149 • Specimen no. 1: Classic partition, composed of 18 mm thick wooden panel;
- 150 • Specimen no. 2: Steel partition, composed of an 18 mm thick plasterboard panel, encased in  
151 1 mm thick steel panel with the edges suitably shaped to allow the connection to the vertical  
152 studs;
- 153 • Specimen no. 3: P85 partition, which is similar to Steel partition, except the internal steel  
154 structure;
- 155 • Specimen no. 4: "Glass" partition, composed of laminated glass panels, which are included  
156 within steel or aluminum frames; these frames are suitably shaped to allow the connection to  
157 vertical studs. A plasterboard panel encased in steel panel is also used on the perimeter to  
158 allow the connection to the vertical track.



159 **Figure 7. View of the tested specimens: a) plan view; b) lateral view**

160 Two different internal steel structure typologies are used. A standard 60 mm thick internal steel  
161 structure is used for specimens no. 1 and no. 2, named P104; specimen no. 3 is characterized by  
162 42 mm thick internal steel structure, named P85. Specimen no. 4 provides both the internal steel  
163 structure typologies; in particular, two partitions (West and South) are composed of laminated glass  
164 panels within a steel frame, with P85 internal structure, while other two partitions (East and North)  
165 are composed of laminated glass panels within an aluminum frame, with P104 internal steel  
166 structure. Partitions with P104 internal steel structure are characterized by 104 mm total thickness,  
167 while the partitions with P85 internal steel structure have a total thickness of 85 mm. A flexible  
168 silicone-based material is installed among the panels, filling the 4 mm gap, in the 3<sup>rd</sup> and 4<sup>th</sup>  
169 specimen, for acoustic and thermal purposes. The tested specimens are characterized by a 6.03 m<sup>2</sup>  
170 area for the East and West walls and 4.74 m<sup>2</sup> for North and South walls. It should be noted that a  
171 door is also installed in both North and South walls. The characteristics of the specimens are  
172 summarized in Table 1.

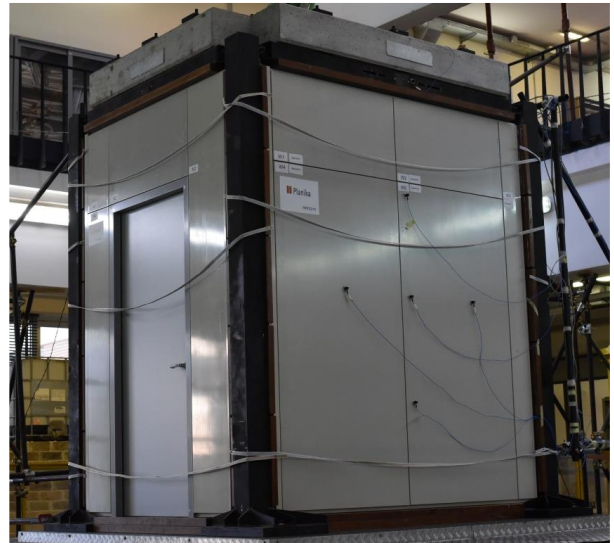
**Table 1. Description of different components for each tested specimen**

	<b>Panels</b>	<b>Steel studs</b>	<b>Steel tracks</b>
<b>Specimen no. 1</b>	18 mm thick wooden panel	35-60-35 mm "equivalent C" section, 1.0 mm thick	60-60-60 mm "U" section, 0.80 mm thick
<b>Specimen no. 2</b>	18 mm thick plasterboard panel, covered with 1 mm thick steel panel	35-60-35 mm "equivalent C" section, 1.0 mm thick	60-60-60 mm "U" section, 0.80 mm thick
<b>Specimen no. 3</b>	18 mm thick plasterboard panel, covered with 1 mm thick steel panel	35-42-35 mm "C" section, 1.2 mm thick	60-42-60 mm "U" section, 0.80 mm thick
<b>N - E</b>	Laminated glass panels within an aluminum frame	35-60-35 mm "equivalent C" section, 1.0 mm thick	60-60-60 mm "U" section, 0.80 mm thick
<b>Specimen no. 4</b>	18 mm thick plasterboard panel, covered with 1 mm thick steel panel	35-42-35 mm "C" section, 1.2 mm thick	60-42-60 mm "U" section, 0.80 mm thick
<b>S - W</b>	laminated glass panels within a steel frame		

Specimen no. 1



Specimen no. 2



Specimen no. 3

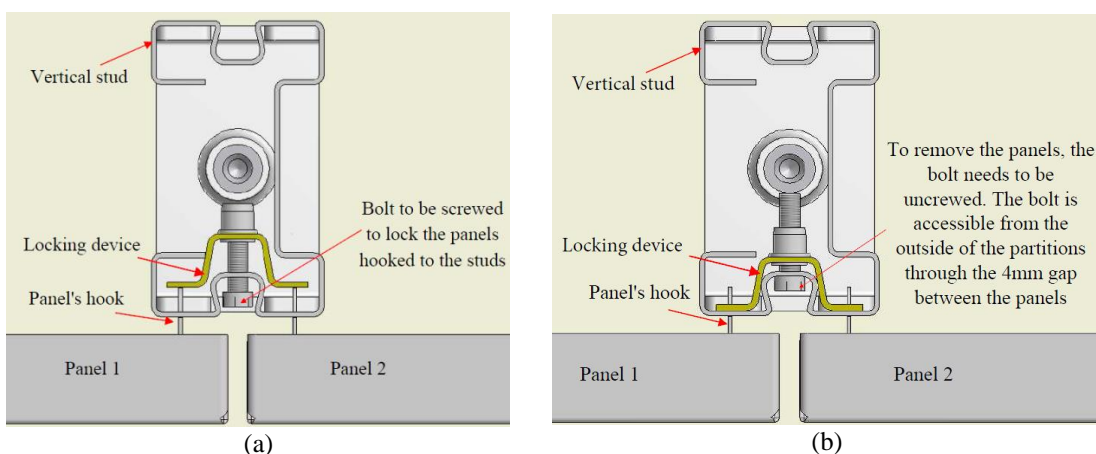


Specimen no. 4

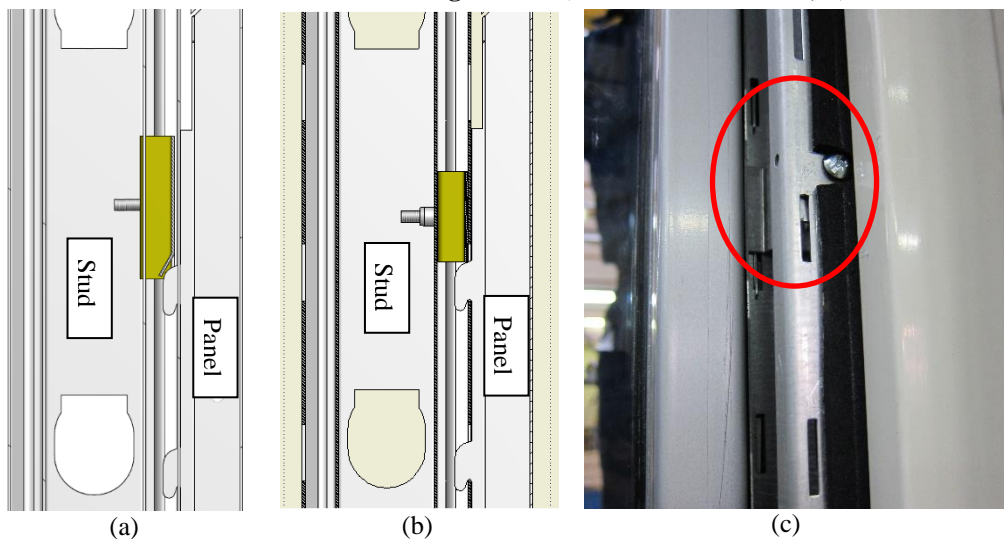
**Figure 8. Global view of the specimens nos. 1-4 (from top left to bottom right)**

176 To avoid the fall of the panels if they overturn, protection ropes are inserted. The presence of such  
177 devices does not influence the seismic behavior of the tested specimens; their presence is merely for  
178 safety during testing. It should be also noted that the influence of return walls on the specimen was  
179 not investigated in this test campaign.

180 An innovative device is introduced in West and South walls of specimens no. 1, 2 and 3, and in all  
181 the walls of Glass partitions. This device aims at avoiding the unhooking of the panels from the  
182 studs. The locking device (Figure 9) is composed of a steel plate with two lateral flaps and a bolt  
183 and it is placed into the stud. It is activated through the tightening of the bolt (Figure 9); once the  
184 bolt is tightened, lateral flaps adhere to the stud, reducing the width of the slots, which house panel  
185 hooks, and preventing the overturning of the panels, if they are subjected to both uplift and out-of-  
186 plane forces. To remove the panels, the bolt needs to be unscrewed; the bolt is accessible from the  
187 outside of the partitions through the 4 mm gap between the panels. For specimen no. 1, the solution  
188 shown in Figure 10a is adopted, with an inclined lower edge of the flaps; in partitions nos. 2-4, a  
189 modified device is adopted (Figure 10b) due to the poor performance of the first solution. The  
190 device was developed by the authors during the tests campaign and is currently patent pending.



191 **Figure 9. Plan view of the in/novative locking device: a) device not activated; b) device activated**



192 **Figure 10. Innovative locking device: a) side view of device used in Classic partitions; b) side view of device used  
193 in the specimens no. 2, 3, 4; c) frontal view**

## 194 **2.2 Input and testing protocol**

195 The input to the shaking table consists of two 30-second time histories representative of a target  
196 ground motion and acting simultaneously along the two horizontal directions; the time histories are  
197 artificially defined so as their response spectra match a target response spectrum derived from  
198 ASCE7-10 [20] force formulation for nonstructural components:

$$F_p = \frac{0.4a_p S_{DS} W_p}{R_p/I_p} \left(1 + 2 \frac{z}{h}\right) \leq 1.6 W_p I_p S_{DS} \quad (1)$$

where  $a_p$  is the floor-to-component amplification factor,  $S_{DS}$  is the design spectral acceleration at short periods,  $W_p$  is the weight of the component,  $R_p$  is the component force reduction factor,  $I_p$  is the importance factor and  $z/h$  is the relative height ratio where the component is installed. The required response spectrum is defined by two spectral accelerations,  $A_{FLX}$  and  $A_{RIG}$ , which assume a component amplification factor  $a_p$  equal to 2.5 and 1, respectively, and  $R_p$  and  $I_p$  equal to 1:

$$A_{FLX} = S_{DS} \left(1 + 2 \frac{z}{h}\right) \leq 1.6 \cdot S_{DS} \quad (2)$$

$$A_{RIG} = 0.4 S_{DS} \left(1 + 2 \frac{z}{h}\right) \quad (3)$$

$A_{FLX}$  is the spectral acceleration acting on flexible components, characterized by a natural frequency ranging from 1.3 Hz to 8.3 Hz, whereas  $A_{RIG}$  is representative of rigid components, i.e. with natural frequency larger than 33.3 Hz. The defined response spectra envelop the target spectrum in the frequency range between 1.3 and 33.3 Hz and assumes a damping value equal to 5% of critical damping. In this range they do not exceed the target spectrum by more than 30%. Furthermore, in cases where it can be shown that no resonance response phenomena exist below 5 Hz, the TRS are required to envelop the target spectrum only down to 3.5 Hz. When resonance phenomena exist below 5 Hz, the TRS are required to envelop target spectrum only down to 75% of the lowest frequency of resonance. Lastly, the peak shake table acceleration shall not be lower than 90% of  $A_{RIG}$ . The time histories are artificially defined according to the procedure included in [21]. The obtained time histories are then filtered with a 0.70 Hz high-pass filter in order not to exceed the displacement and velocity limitations of the earthquake simulator. Results are shown in Figure 11. The procedure has been executed for  $S_{DS} = 1.00g$ ; the accelerograms are then scaled to reach several shaking intensities.

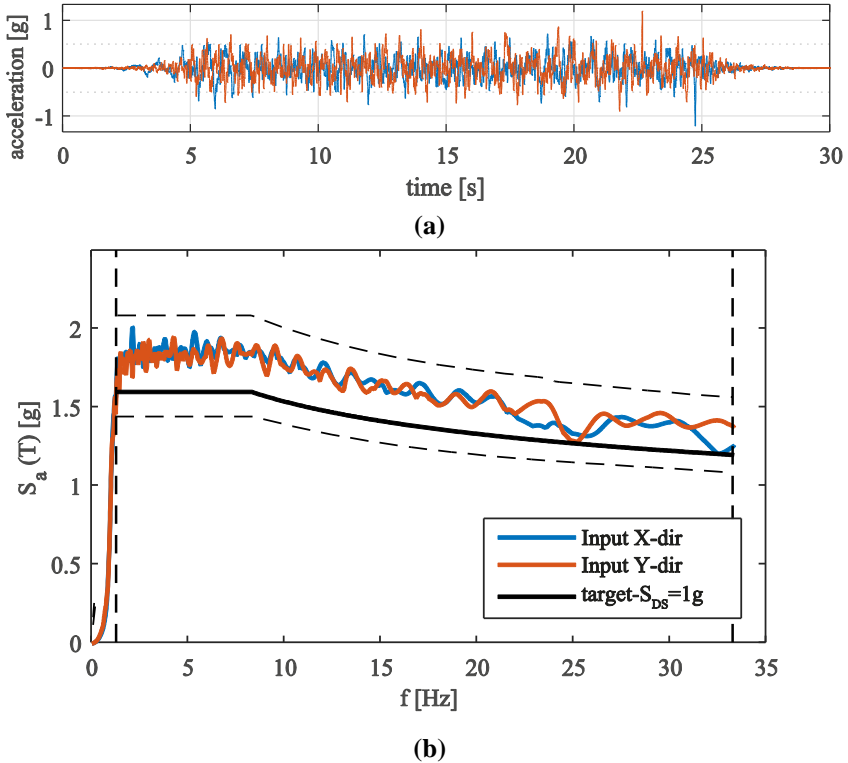
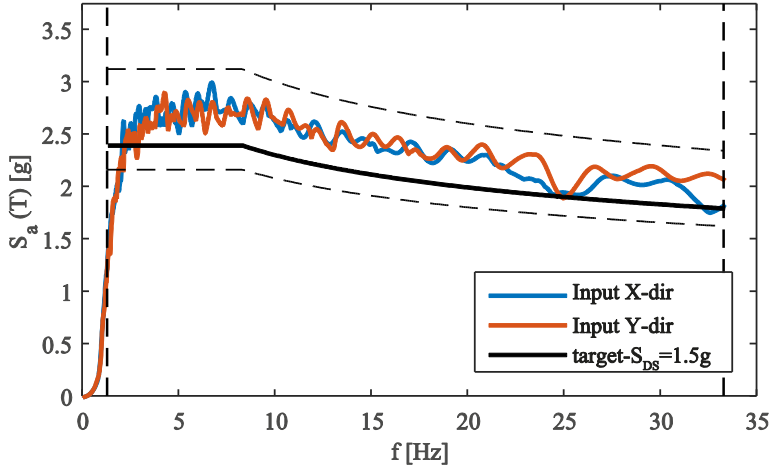


**Figure 11. Input time histories and spectra for  $S_{DS}$  equal to 1.00 g: (a) acceleration time-history - X direction (blue) and Y direction (red); (b) input accelerogram spectra and matching frequency range (vertical dashed line)**

The test frame is designed for a bidirectional input motion characterized by a 2.0 g spectral acceleration, which corresponds to 1.0% interstory drift ratio. In case unidirectional input motion is employed, larger acceleration and interstory drift can be obtained without damaging the test setup. An additional couple of time histories have therefore been generated, to be used for unidirectional

227 tests (Figure 12). This couple of accelerograms is filtered with a 1.32 Hz high-pass filter in order to  
 228 not exceed displacement limitations of the adopted instrumentation. The corresponding couple of  
 229 spectra is still abiding to the prescriptions above on spectrum matching, considering the expected  
 230 natural frequency of the tested components.



231 **Figure 12. Input accelerogram spectra, target spectrum and its limits (dashed line) for  $S_{DS}$  equal to 1.50 g**

232 The input levels range from  $S_{DS} = 0.05 g$  to  $S_{DS} = 1.50 g$  in order to generalize the execution of  
 233 the test, being representative of a large range of earthquake intensities. As mentioned above,  
 234 unidirectional tests should be performed in case an interstory drift larger than 1.0% is expected in  
 235 order to ensure the integrity of the test frame. The test campaign provides shakings increasing  
 236 intensity with 0.10 g steps. In case damage is observed, a shaking characterized by a 0.05 g lower  
 237 intensity is applied, in order to find a more accurate threshold of the seismic intensity which causes  
 238 such a damage. For example in specimen no. 2, a test characterized by 0.25g  $S_{DS}$  intensity value is  
 239 performed after a 0.30g  $S_{DS}$  test, since a given damage is recorded at 0.30 g  $S_{DS}$  value. A low-  
 240 intensity random vibration is performed after each test, in order to monitor the dynamic properties  
 241 of the test setup throughout the different test campaigns. Finally, it should be underlined that the use  
 242 of shake table tests is justified to test internal partitions due to the following reasons [9]:

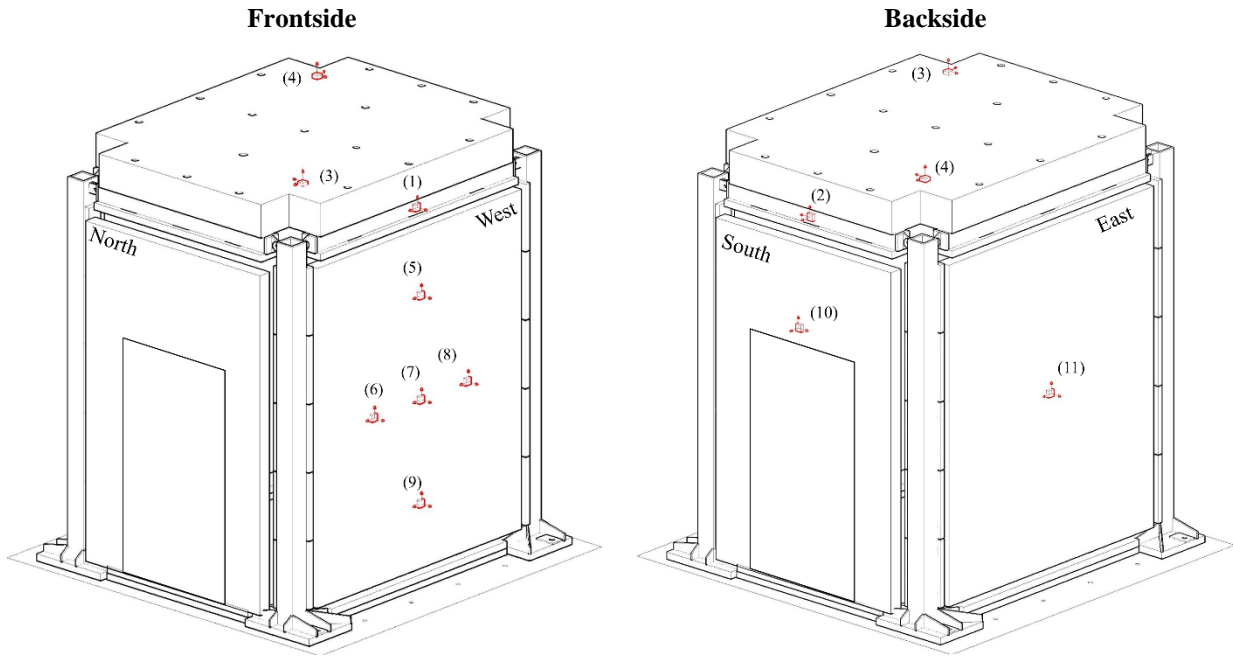
- 243 • internal partitions are mainly displacement sensitive components; however, out-of-plane  
 244 acceleration can induce the collapse of these components;
- 245 • the use of a flexible test frame, subjected to the defined input motions, allows investigating  
 246 the behavior of the tested component at a given level of in-plane relative displacement  
 247 demand.

### 248 **2.3 Instrumentation**

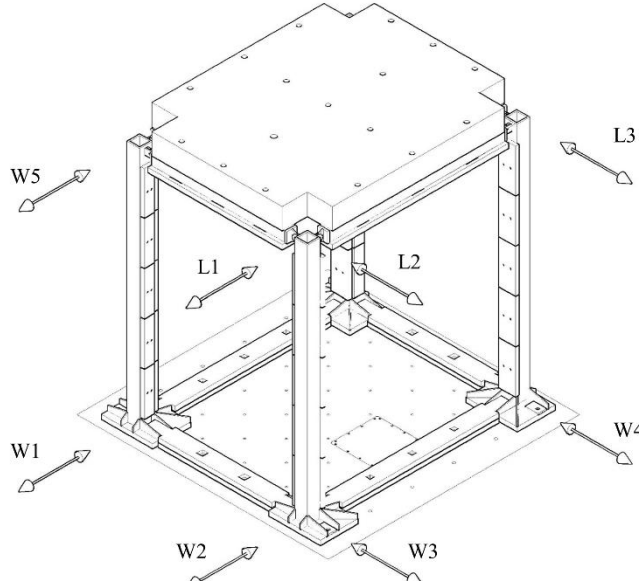
249 Tri-axial accelerometers and displacement laser sensors are used to monitor the response of both the  
 250 test frame and the specimen. One accelerometer, placed inside the shake table, measures the input  
 251 accelerations in both directions. Eleven accelerometers are also arranged in order to monitor the  
 252 acceleration at different locations of the setup, as shown in Figure 13. Two accelerometers, (1) and  
 253 (2) in Figure 13, are installed on two orthogonal beams; other two instruments, (3) and (4) in Figure  
 254 13, are arranged on the concrete slab above the test frame; seven accelerometers are installed on the  
 255 partitions, in order to investigate their out-of-plane behavior. Five accelerometers are placed on the  
 256 West wall; one accelerometer, (7) in Figure 13, is placed at the center of the wall, while the other  
 257 four instruments are installed along the vertical and the horizontal directions of the accelerometer  
 258 (7), in order to evaluate the acceleration distribution of the partition along two orthogonal  
 259 directions. Other two accelerometers are installed: the first one at the center of the East wall, the  
 260 second one at the South wall, above the door.

261 Displacement laser sensors are also employed (Figure 14); in particular five short-range laser  
 262 sensors (denoted with "W" prefix in Figure 14) and three long-range laser sensors (denoted with

263 “L” prefix in Figure 14) are used. Sensors are installed in order to evaluate the absolute and relative  
 264 displacements of columns in both the horizontal directions.



265 **Figure 13. Accelerometer positions on both the steel test setup and the specimen**



266  
 267 **Figure 14. Laser positions**

268 **3 RESULTS AND DISCUSSION**

269 **3.1 Summary of the results**

270 Bidirectional and unidirectional shaking tests are performed along two horizontal directions. In case  
 271 unidirectional motion is selected, two different tests are performed in the two orthogonal directions.  
 272 The results of the different test campaigns are summarized in Table 2, which includes for each test:  
 273 (a) the reference SDS intensity values; (b) peak acceleration at the table level in X and Y directions  
 274 (Figure 7a) recorded by the accelerometer inside the table; (c) peak acceleration at the roof of the  
 275 test frame in X and Y directions recorded by accelerometers placed either on the roof (acc. no. 3  
 276 and 4 in Figure 13) or on horizontal beams (acc. no. 1 and 2); (d) peak relative displacements,  
 277 evaluated as the difference between absolute displacements at the roof and at the table. The  
 278 displacements are evaluated using the laser recordings at the top (W5, L1, L2 and L3 in Figure 14)

279 and at the base of the test frame (W1, W2, W3 and W4 in Figure 14); (e) maximum interstory drift  
 280 ratios, evaluated as the ratio between maximum relative displacements and the height of the test  
 281 setup, equal to 2.74m. Values related to unidirectional tests are marked by an asterisk in Table 2.

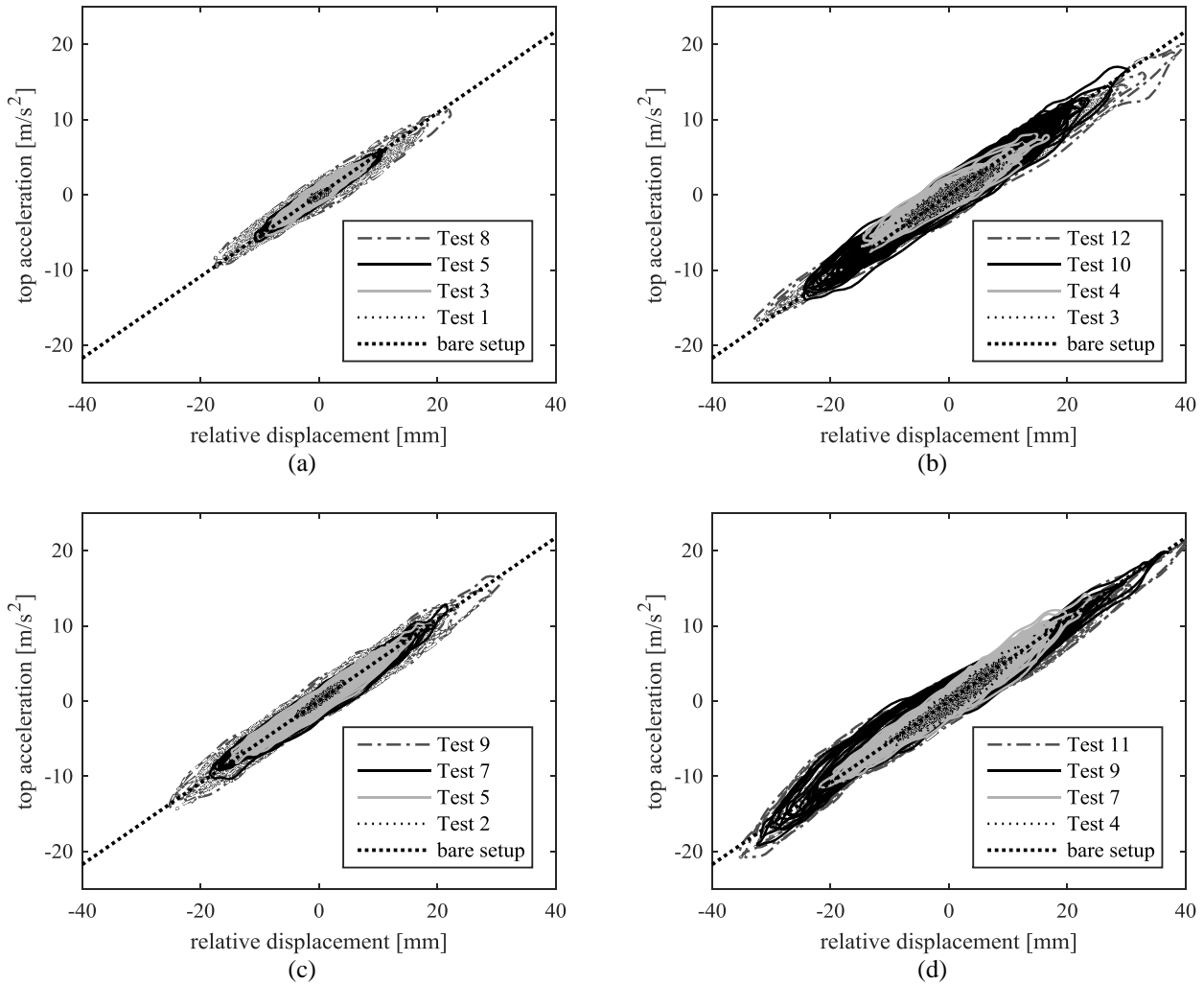
282 **Table 2. Summary of the recorded quantities for each test of the different campaigns. Unidirectional tests are**  
 283 **denoted with an asterisk**

		Test ID											
		1	2	3	4	5	6	7	8	9	10	11	12
		<b>Classic partition</b>											
	<b>Sds (g)</b>	0.05	0.10	0.20	0.30	0.25	0.35	0.40	0.50	-	-	-	-
<b>Table</b>	<b>X (g)</b>	0.06	0.12	0.25	0.36	0.30	0.41	0.46	0.58	-	-	-	-
	<b>Y (g)</b>	0.07	0.11	0.24	0.35	0.31	0.40	0.46	0.56	-	-	-	-
<b>Acc. 1</b>	<b>X (g)</b>	0.12	0.22	0.42	0.59	0.49	0.67	0.81	1.01	-	-	-	-
	<b>Y (g)</b>	0.13	0.25	0.56	0.81	0.66	0.91	1.01	1.23	-	-	-	-
<b>L3-W4</b>	<b>X (mm)</b>	2.63	5.12	9.55	10.7	7.10	9.49	12.3	16.1	-	-	-	-
	<b>Y (mm)</b>	2.49	4.76	9.38	14.9	11.3	15.7	17.8	22.2	-	-	-	-
<b>W5-W1</b>	<b>X (%)</b>	0.10	0.19	0.35	0.39	0.26	0.35	0.45	0.59	-	-	-	-
	<b>Y (%)</b>	0.09	0.17	0.34	0.54	0.41	0.57	0.65	0.81	-	-	-	-
		<b>Steel partition</b>											
	<b>Sds (g)</b>	0.05	0.10	0.20	0.30	0.25	0.35	0.40	0.50	0.60	0.70	0.825*	0.975*
<b>Table</b>	<b>X (g)</b>	0.06	0.12	0.25	0.38	0.31	0.42	0.49	0.58	0.68	0.77	0.91*	1.04*
	<b>Y (g)</b>	0.06	0.12	0.24	0.37	0.30	0.41	0.46	0.59	0.71	0.86	1.06*	1.20*
<b>Acc. 1</b>	<b>X (g)</b>	0.15	0.21	0.42	0.61	0.54	0.71	0.83	1.07	1.32	1.59	1.91*	2.22*
	<b>Y (g)</b>	0.15	0.30	0.58	0.85	0.69	0.89	1.02	1.29	1.51	1.73	1.83*	2.04*
<b>L2-W3</b>	<b>X (mm)</b>	3.35	4.16	6.00	9.40	8.28	11.6	13.4	16.9	20.5	24.4	30.9*	34.6*
	<b>Y (mm)</b>	2.83	5.65	10.0	14.0	11.3	14.1	16.9	21.9	26.9	30.2	33.9*	39.4*
<b>W5-W1</b>	<b>X (%)</b>	0.12	0.15	0.22	0.34	0.30	0.43	0.49	0.62	0.75	0.89	1.13*	1.26*
	<b>Y (%)</b>	0.10	0.21	0.37	0.51	0.41	0.51	0.62	0.80	0.98	1.10	1.24*	1.44*
		<b>P85 partition</b>											
	<b>Sds (g)</b>	0.05	0.10	0.20	0.30	0.40	0.35	0.50	0.60	0.70	-	-	-
<b>Table</b>	<b>X (g)</b>	0.06	0.12	0.25	0.38	0.50	0.42	0.60	0.69	0.79	-	-	-
	<b>Y (g)</b>	0.07	0.12	0.24	0.36	0.48	0.42	0.59	0.76	0.82	-	-	-
<b>Acc. 1</b>	<b>X (g)</b>	0.11	0.19	0.37	0.65	0.91	0.80	1.11	1.23	1.41	-	-	-
	<b>Y (g)</b>	0.13	0.27	0.53	0.78	1.05	0.92	1.31	1.56	1.69	-	-	-
<b>L3-W4</b>	<b>X (mm)</b>	2.37	3.24	5.85	10.4	13.8	11.6	16.6	19.4	22.3	-	-	-
	<b>Y (mm)</b>	2.39	4.51	8.86	13.2	17.8	14.9	21.7	26.2	30.9	-	-	-
<b>W5-W1</b>	<b>X (%)</b>	0.09	0.12	0.21	0.38	0.50	0.43	0.60	0.71	0.81	-	-	-
	<b>Y (%)</b>	0.09	0.16	0.32	0.48	0.65	0.54	0.79	0.96	1.13	-	-	-
		<b>Glass partition</b>											
	<b>Sds (g)</b>	0.05	0.10	0.20	0.30	0.40	0.50	0.60	0.70	0.825*	0.975*	1.125*	-
<b>Table</b>	<b>X (g)</b>	0.06	0.12	0.25	0.37	0.48	0.59	0.69	0.77	0.94*	1.05*	1.19*	-
	<b>Y (g)</b>	0.06	0.12	0.24	0.36	0.47	0.59	0.71	0.81	0.98*	1.20*	1.63*	-
<b>Acc. 4</b>	<b>X (g)</b>	0.13	0.21	0.42	0.63	0.89	1.16	1.41	1.63	1.89*	2.18*	2.51*	-
	<b>Y (g)</b>	0.13	0.25	0.46	0.75	1.03	1.27	1.45	1.63	1.75*	2.02*	2.30*	-
<b>L3-W4</b>	<b>X (mm)</b>	1.96	3.03	6.50	9.83	13.0	17.6	21.1	24.0	30.7*	33.0*	37.8*	-
	<b>Y (mm)</b>	1.97	4.54	7.85	12.3	16.5	20.0	24.0	28.4	31.7*	37.1*	43.0*	-
<b>W5-W1</b>	<b>X (%)</b>	0.07	0.11	0.24	0.36	0.47	0.64	0.77	0.88	1.12*	1.20*	1.38*	-
	<b>Y (%)</b>	0.07	0.17	0.29	0.45	0.60	0.73	0.88	1.04	1.16*	1.35*	1.57*	-

284 Maximum values of acceleration recorded on the roof in both X and Y directions are larger than  
 285 peak table accelerations due to dynamic amplification; in particular, the mean dynamic  
 286 amplification, evaluated as the ratio between peak acceleration at roof and peak table acceleration,  
 287 is in the range 2 – 2.15 and 1.8 – 1.9 for the different specimens in Y and X direction,  
 288 respectively. The amplification leads to acceleration values larger than 2.0 g at the roof for Steel  
 289 and Glass partitions, 1.0 g for Classic partition, and 1.5 g for P85 partition. The dynamic  
 290 amplification is compatible with the target value of 1.9, from the spectra in Figure 11b. The  
 291 maximum interstory drift value (1.57% in Y direction) is recorded for the 4<sup>th</sup> specimen, because the  
 292 integrity of the partition system allows executing the test at such a large Sds intensity value.  
 293

294 However, values up to 0.8% drift, representative of a moderate earthquake intensity level, are  
295 recorded for all specimens.

296 In order to analyze the partition behavior and its contribution to the global behavior of the test  
297 setup, the top acceleration, representative of the total inertia force, is plotted versus the relative  
298 displacement for different intensity levels; for the sake of both brevity and clarity, only the results  
299 of some tests in Y direction are shown in Figure 15. A dotted black line denotes the behavior of the  
300 bare test frame based on its natural frequency. Hysteresis loops in X direction exhibit a similar  
301 trend.



302 **Figure 15. Top acceleration versus relative displacement plot for different seismic tests in Y direction: a) Classic  
303 partition; b) Steel partition; c) P85 partition; d) Glass partition**

304 From the analysis of the hysteretic curves it can be noted that there is a negligible interaction  
305 between the partitions and the hosting structure; this outcome confirms that the partitions do not  
306 contribute to the lateral stiffness even for large displacements, since the hysteresis loops are aligned  
307 with the behavior of the bare test frame.

308 Maximum dynamic amplification on the component and acceleration distribution of the partition  
309 along two orthogonal directions are also obtained using the accelerometers placed on the panels.  
310 The amplification factor for out-of-plane acceleration on walls is typically included between 2 and 3  
311 for all the different partition walls. These value suggest that the amplification factor is typically well  
312 predicted by the 2.5 factor suggested in ASCE 7 for flexible components [20]. The acceleration on  
313 the panels in the out-of-plane direction is almost constant at different location characterized by the  
314 same height (accelerometers no. 6 and 8 vs accelerometer no. 7); this suggests that the partitions  
315 deform in the out-of-plane mainly along the vertical plane, whereas negligible deformations are  
316 recorded in the horizontal plane. Some discrepancies are recorded in case accelerometers no. 5 and

317 9 are compared to accelerometer no. 7; out-of-plane accelerations at the top and at the bottom of the  
318 panel are about 1.2 and 0.8 times the acceleration at the center of the partition, respectively. This  
319 result is expected since the panel is subjected on the top to an acceleration which is larger, i.e.  
320 almost doubled, than the acceleration at the base of the partition.

### 321 **3.2 Damage description and fragility assessment**

322 In this study three damage states (DS) are considered for the seismic response definition of the  
323 partitions, i.e. minor damage state DS1, moderate damage state DS2 and major damage state DS3.  
324 Minor damage state achievement implies the need to slightly repair the specimen, in order to restore  
325 its original condition. Moderate damage state achievement, instead, implies that the nonstructural  
326 component is damaged so that it should be partially replaced. Major damage state implies that the  
327 damage level is such that either the partition needs to be totally replaced or the life safety is not  
328 ensured. The damage state definitions and their consequences are included in Table 3; they are  
329 based on the definition given by Taghavi and Miranda [3]. In particular the correlation between  
330 each damage state and the loss is given in terms of the three Ds [22]: (a) human casualties (Deaths),  
331 (b) direct economic loss due to the repair or replacement of the nonstructural component (Dollars)  
332 and (c) occupancy or service loss (Downtime). After each shaking level, damage is observed by  
333 inspecting the physical conditions of the components and an appropriate damage table is compiled.  
334 In particular, the damage level required to reach a given damage state is indicated for each  
335 component of the partition; obviously, the damage state is the maximum between the different  
336 damage states recorded in each component. Finally, it should be noted that some damage typologies  
337 can be observed only at the end of each test, after dismantling the specimen.

338 Recorded damage is similar for all the specimens. In particular the following damage typologies are  
339 recorded:

- Detachment and fall of panels (not recorded for Glass partitions), with increasing intensity as the demand increases (Figure 16a-c). For low-intensity shakings the panels typically detaches on one side, acting as a door (e.g. panel above the door in Figure 16b), without overturning; out-of-plane slight rotation of the panels are therefore observed.
- Detachment of the flexible silicone-based material (Figure 16d-e), which fills the gap among the panels (for the 3<sup>rd</sup> and 4<sup>th</sup> specimen) and the gap among glass panels and steel frame (Figure 16f, 4<sup>th</sup> specimen).
- Local plastic deformations of panel hooking system (Figure 16g-h), due to relative displacement between panels and studs.
- Local plastic deformations of the extremities of studs (Figure 16i, only for P85 internal steel structure).
- The correlation between the damage state (DS) and the interstory drift ratio (IDR) is shown in Table 4 for partitions without the innovative device described in Section 2.1 (Figure 9- Figure 10), named standard partitions. It should be reminded that the first three test campaigns provide that two standard specimens, i.e. North and East partitions, and two innovative specimens, i.e. South and West partitions, are tested simultaneously. The fourth test campaign, instead, provides that four innovative specimens characterized by two different panel typologies are tested at the same time. Different damage states are simultaneously reached for some tests, hence the IDR values required to attain different damage states are coincident, e.g. DS 2 and DS 3 in steel partitions (Table 4). When no damage is recorded until the end of the test, it is reported that the IDR value causing a given damage state is larger than the maximum IDR measured for the specimen.

**Table 3. Damage scheme for the correlation between the recorded damage in each component of the partition and the attained damage state**

	<b>DS 1</b>	<b>DS 2</b>	<b>DS 3</b>
<b>Dollars</b>	Need to repair or replace a percentage of specimens larger than 10%	30%	50%
<b>Downtime</b>	-	Moderate (1-2 days)	Significant ( $\geq 3$ days)
<b>Death</b>	-	Limited	Significant
<b>Component</b>	<b>DS 1</b>	<b>DS 2</b>	<b>DS 3</b>
Wood panels	Out-of-plane slight rotation of the panels, local plastic deformations of the anchoring system to the studs	Fall of a single panel with negligible damage, need to replace anchoring systems	Fall of more than a single panels, wide cracks ( $>0.3$ mm) in the panels
Steel and glass panels	Out-of-plane slight rotations of the panels, local plastic deformations of the anchoring system to the studs	Fall of a single panel with negligible damage	Fall of more than a single panel, cracks in the panel, irreparable damage of the anchoring system
Steel studs	Repair of the PVC gaskets	Local plastic deformations, slight deformations due to buckling ( $d/h < 1/200$ )	Collapse due to instability, significant out-of-plane deformations ( $d/h \geq 1/200$ ), extensive plastic deformation
Horizontal element	Detachment of the locking lever, repair of the PVC gaskets	Local plastic deformations, minor impact, slight deformations due to buckling ( $d/h < 1/200$ )	Significant out-of-plane deformations ( $d/h \geq 1/200$ ), extensive plastic deformation, collapse of the locking lever
Steel tracks	Local detachment of the neoprene pad	Local plastic deformations of the section, significant detachment of the neoprene pad	Permanent displacements, significant plastic deformations of the section, collapse due to instability

As shown in Table 4, no damage is recorded up to 0.50% for all standard partitions, except in Y direction for the 1<sup>st</sup> specimen. Standard partitions in X direction, characterized by a door, generally exhibit a better behavior than the ones in Y direction. The damage states occur for interstory drifts in the range 0.41-0.65 for DS1, due to the out-of-plane slight rotation of the panels, and in the range 0.51-0.81 for DS2, for the fall of a single panel, and DS3, for the fall of more panels.

The correlation between the damage state (DS) and the interstory drift ratio (IDR) for innovative partitions is also shown in Table 4, to evaluate the influence of the innovative device. The seismic performance of all the partitions improves after the introduction of the innovative device, especially for the walls without a door. No damage is recorded for all the innovative partitions in X direction, while only a minor damage state is recorded in Y direction for Classic partition and for the specimens with P85 internal steel structure. The device used for Classic partition exhibits a poor efficiency; the recorded damage in the innovative partition of the 1<sup>st</sup> specimen is, in fact, due to unhooking of the panels, while the device used in the other specimens avoids this failure mechanism. Large increase of collapse IDR is recorded with the introduction of the innovative device, up to IDR larger than 1.44% for Steel partition in Y direction. However, it can be noted that all the innovative partitions do not exhibit damage for interstory drift smaller than the 0.5% drift limitation included in Eurocode 8 [23].



383  
384  
385  
386  
Figure 16. Recorded damages: (a) detachment and fall of Classic panels, (b) P85 panels, (c) Steel panels; (d)  
detachment of the flexible silicone-based material in P85 partition and (e) Glass partition; (f) detachment of the  
silicone-based material in glass panel; (g) deformed glass panel hooking system with steel frame and (h)  
with aluminum frame; (i) deformed P85 stud

387  
388  
**Table 4. Interstory drift ratio required to attain the considered damage states (DS) for standard and innovative  
partitions**

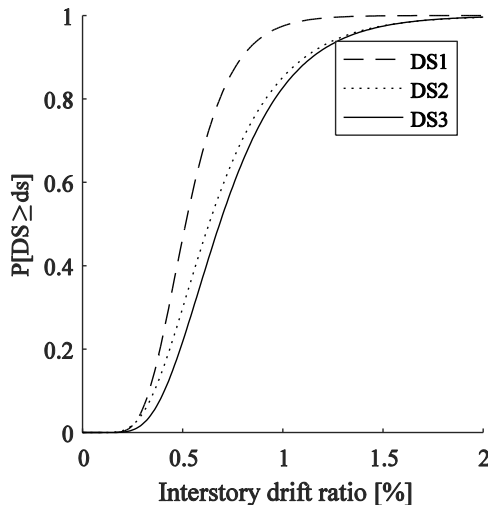
Specimen	Direction	Interstory drift ratio (%)					
		Standard partition			Innovative partition		
		DS1	DS2	DS3	DS1	DS2	DS3
Classic partition	X	>0.59	>0.59	>0.59	>0.59	>0.59	>0.59
	Y	0.41	0.54	0.65	0.54	>0.81	>0.81
Steel partition	X	1.13	1.26	>1.26	>1.26	>1.26	>1.26
	Y	0.512	0.514	0.514	>1.44	>1.44	>1.44
P85 partition	X	0.81	0.81	>0.81	>0.81	>0.81	>0.81
	Y	0.65	0.96	0.96	1.13	1.13	>1.13

389 For the 4<sup>th</sup> specimen, the innovative device is used in all the walls: in Table 5 the correlation  
 390 between DS and IDR is shown for the two typologies of glass partitions, to evaluate their different  
 391 seismic behavior. As clearly shown in the Table 5, no significant damage is recorded for glass  
 392 panels within a steel frame, while glass panels within an aluminum frame are undamaged at the end  
 393 of the tests, despite the high level of experienced horizontal accelerations. The seismic performance  
 394 of glass panels with P104 internal steel structure is better than that of the panels with P85 internal  
 395 steel structure; in fact, during the dismantling, P85 internal structure exhibits local plastic  
 396 deformations, while the P104 one remains undamaged (Figure 16i).

397 **Table 5. Interstory drift ratio required to attain the considered damage states (DS) for glass partitions**

Specimen	Direction	Interstory drift ratio (%)					
		Glass panel within a steel frame and P85 internal steel structure			Glass panel within an aluminum frame and P104 internal steel structure		
		DS1	DS2	DS3	DS1	DS2	DS3
Glass Partition	X	0.36	>1.38	>1.38	>1.38	>1.38	>1.38
	Y	1.35	>1.57	>1.57	>1.57	>1.57	>1.57

398 The data in Table 4 can be used to estimate fragility curves for the tested partition walls (Figure 17).  
 399 The evaluation is performed according to the method “A” suggested by Porter et al. [24] and  
 400 applied in [11, 25]. Fragility curves are assessed only for standard temporary partitions (Table 4)  
 401 oriented along Y direction, i.e. the “wide” specimens, since all the three different damage states are  
 402 recorded only for these specimens.



Damage state	$x_m$ [%]	$\beta$
DS1	0.515	0.340
DS2	0.631	0.441
DS3	0.685	0.403

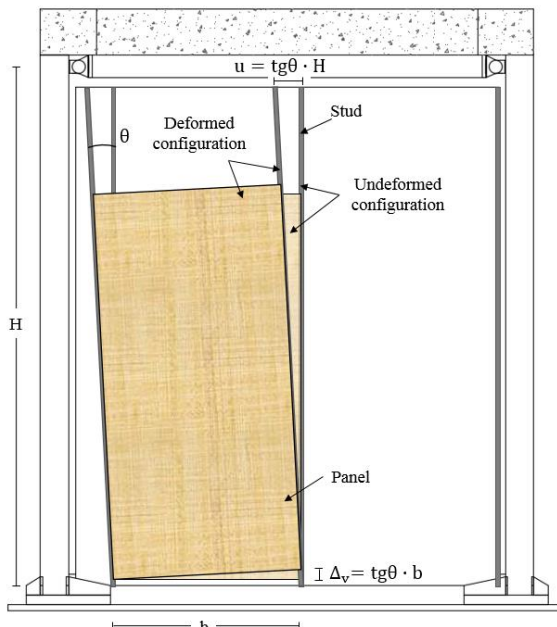
404 **Figure 17. Fragility curves for standard temporary partition walls**

405 The median values  $x_m$  of the fragility curves are typically smaller than the corresponding values  
 406 assessed in [11, 18] for plasterboard partition walls, particularly for DS2 and DS3. The logarithmic  
 407 standard deviation  $\beta$  of the fragility curves are, instead, comparable to the ones in [11, 18]. It is  
 408 important to underline that the fragility curves for innovative specimens would be significantly  
 409 different, with a much larger median value. Indeed, these specimens show none or negligible  
 410 damage for interstorey drifts larger than 1% (Table 4 - Table 5).

### 412 **3.3 Comments on the failure mechanism**

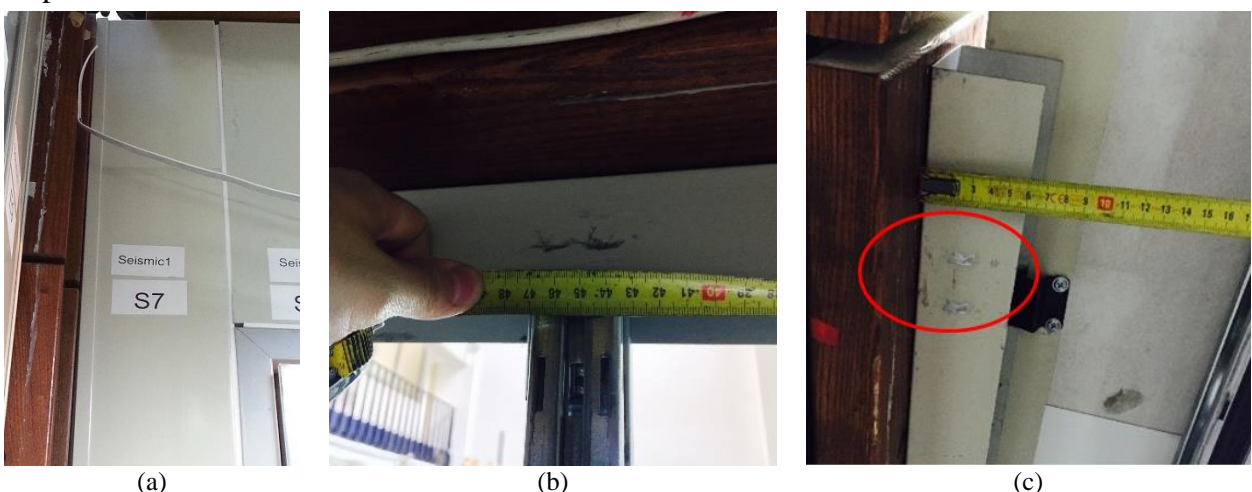
413 The definition of the innovative device is based on the identification of the reason why the failure  
 414 mechanism, i.e. the overturning of the panels, occurs. The deformed configuration of the specimen  
 415 is therefore investigated (Figure 18). Each panel behaves like a rigid block with two unrestrained  
 416 degrees of freedom, i.e. vertical translation in the partition plan and rotation around the out-of-plane  
 417 axis, due to its construction technology. A given relative displacement  $u$  causes a rigid rotation of  
 418 the vertical studs. The panel, which is attached to two vertical studs, rigidly rotates about one of its  
 419 base corners, causing the uplift of the panel on one side ( $\Delta_V$  in Figure 18).

420 For standard partitions, without unhooking device, panel uplift may cause the unhooking of the  
 421 panel from the vertical stud, if the vertical displacement of the panel is larger than the 4 mm length  
 422 of the hooks housed in the slotted holes of the stud. For example, the 1 m wide central panel is  
 423 subjected to a vertical displacement of 5 mm ( $\Delta_v = \tan\theta \cdot b = 0.005 \cdot 1\text{m}$ ) when the interstory drift  
 424 is equal to 0.5% (Figure 18). Once the panel is unhooked, the out-of-plane force acting on the  
 425 partition causes the panel to move outwards and, eventually, to fall to the ground.



426  
 427 **Figure 18. Partition rigid-body mechanism for moderate displacement demand level**

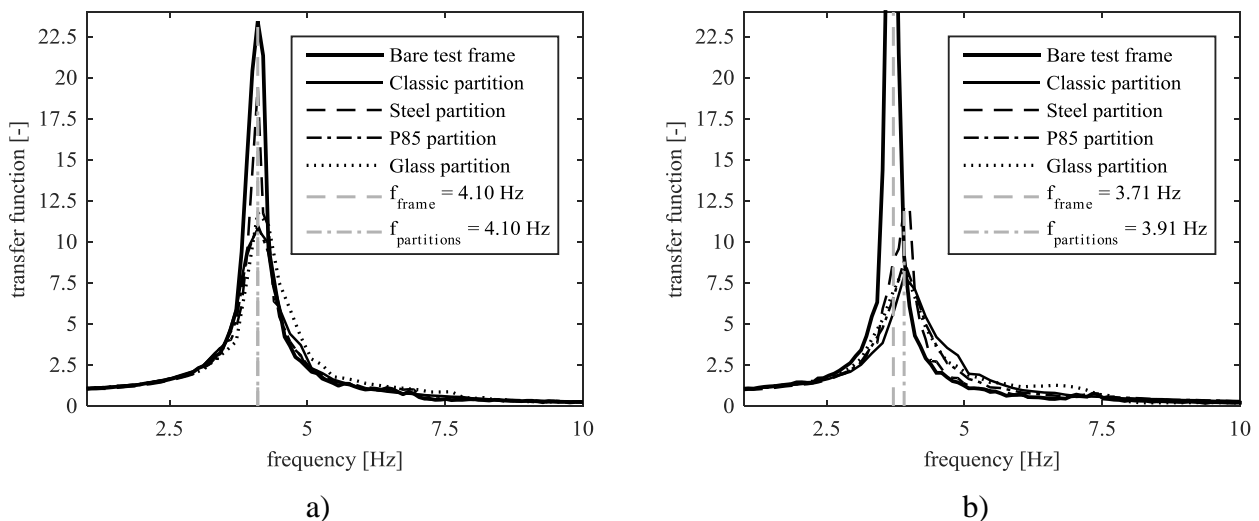
428 Visible signs (Figure 19), which demonstrate the relative displacement between different elements  
 429 of the partition and confirm the rigid mechanism in Figure 18, are denoted at the end of each test  
 430 after dismantling the partitions. In particular, permanent displacement of the stud and consequent  
 431 decrease of partition-to-perimeter gap (Figure 19a) is exhibited, due to the relative displacement  
 432 between studs and horizontal tracks. Moreover, localized damage of tracks, due to the frictional  
 433 sliding between panels and horizontal (Figure 19b) and vertical tracks (Figure 19c) is also denoted.  
 434 Finally, it can be concluded that the behavior of the tested partition walls is mainly influenced by  
 435 the spacing among studs, whereas the total width of the specimen should not significantly influence  
 436 its performance.



437  
 438 **Figure 19. Signs after dismantling of partitions: decrease of partition-to-perimeter gap (a); localized damage of  
 horizontal (b) and vertical (c) tracks**

439 **3.4 Dynamic properties of the test setup**

440 The transfer function method is used for the dynamic identification of the pre-damaged test setup,  
 441 both bare and infilled, in order to evaluate the natural frequency of the bare test frame in both the  
 442 horizontal directions and the influence of the specimens on the dynamic properties of the test setup.  
 443 Before the execution of the test campaign, low-intensity random excitations are selected as input  
 444 motions for the bare test frame; the transfer function method is applied between the base and the top  
 445 acceleration time histories (Figure 20). Frequency values of 4.10 Hz and 3.71 Hz, i.e. 0.24 s and  
 446 0.27 s, denoted by the peak in the transfer curves, are obtained in X and Y directions, respectively.  
 447 After the specimens are installed within the test frame and before executing the shake table tests, a  
 448 random vibration is also applied in both the horizontal directions in order to measure the influence  
 449 of the specimens on the natural frequency of the test setup. As shown in Figure 20, the “infilled”  
 450 natural frequency of the test setup does not change in X direction, while it slightly increases in Y  
 451 direction; it can be therefore concluded that the tested partitions do not significantly interfere with  
 452 the hosting structure.



453 **Figure 20. Transfer functions between base and top acceleration time histories for a low-intensity random**  
 454 **vibration applied to both bare and infilled test setups (a) in X direction and (b) in Y direction**

455 The peak value of the bare setup transfer function, equal to 42.0, is not visible in Figure 20 for the  
 456 sake of clarity. Figure 20 also shows that the damping ratio of the test setup increases after the  
 457 addition of the partition within the test frame, especially for Y direction, causing a beneficial effect  
 458 in the dynamic response.

459 The evaluation of the damping ratio as well as the natural frequency during the test campaign is  
 460 investigated in order to correlate the occurred damage with the dynamic features of the specimen.  
 461 The transfer function method and the procedure proposed by Hashemi and Mosalam [26] are  
 462 implemented in order to evaluate the natural frequency of the test setup. The transfer function  
 463 method is applied between the base and the top acceleration time histories recorded during the low-  
 464 intensity random vibrations performed after the different seismic tests. The procedure proposed by  
 465 Hashemi and Mosalam consists in evaluating the average values of stiffness  $k$  and damping  
 466 coefficient  $b$  of an equivalent single degree of freedom system from the dynamic equilibrium. In  
 467 particular, the values of stiffness  $k$  and damping coefficient  $b$  are those for which the error in  
 468 evaluating the dynamic equilibrium equation is minimized for each time instant. The natural  
 469 frequencies are evaluated starting from the average stiffness. The procedure is applied to the  
 470 different seismic tests at different SDS levels.

471 The natural frequency during the seismic tests for the different partitions is evaluated according to  
 472 (a) the transfer function method, (b) the natural frequency computed according the Hashemi and  
 473 Mosalam procedure (Figure 21). Natural frequency trends show an almost constant envelope, thus  
 474 denoting the absence of damage in the test setup. Moreover, recorded natural frequencies are in the

vicinity of the bare frame natural frequencies in both X and Y direction, confirming the negligible interaction of the tested specimen with the test frame. Hashemi and Mosalam procedure agrees with the “standard” transfer function method with a slightly underestimation. Moreover, such a method tends to significantly underestimate the natural frequency for low-intensity tests, probably due to the noise recorded by the accelerometers.

The equivalent damping ratio  $\xi$  can be evaluated according to following relationship assuming dissipation exclusively viscous:

$$\xi = \frac{W_D}{4\pi E} \quad (4)$$

where  $W_D$  is the dissipated energy for cycle (area enclosed within each hysteresis cycle), and  $E$  is the associated elastic energy [27]. This procedure is applied to each hysteresis cycle of each test. The median value of damping coefficient is shown in Figure 22 for each test. The damping ratio  $\xi$  is also evaluated from the procedure proposed by Hashemi and Mosalam [26] according to

$$\xi = \frac{b}{2\sqrt{k \cdot m}} \quad (5)$$

where  $k$  is the lateral stiffness,  $m$  is the mass of the equivalent single degree of freedom system and  $b$  is evaluated according to the above mentioned method. The damping ratio is evaluated for the different partitions according to both energetic method and the procedure proposed by Hashemi and Mosalam (Figure 22). The damping ratio is in the range 5–10%. A significant increase in the damping ratio is exhibited for all the specimens compared to the bare test setup damping ratio, probably due to the friction developed by vertical studs, that slide with respect to the horizontal tracks, and by panels hooking system inside the slotted holes in vertical studs. An additional contribution is given by the flexible silicone-based material installed among the panels for the 3<sup>rd</sup> and 4<sup>th</sup> specimen. Good agreement between energetic method and Hashemi and Mosalam procedure is shown in Figure 22, with the exception of the low-intensity vibration range, probably due to the noise recorded by the accelerometers. The damping ratio is not influenced by the intensity of the shaking for the 4<sup>th</sup> specimen in both directions. For the other specimens, the damping ratio slightly decreases for the final tests, once the panels are detached, since the damping due to the relative displacement between panels and studs and panels and vertical tracks vanishes.

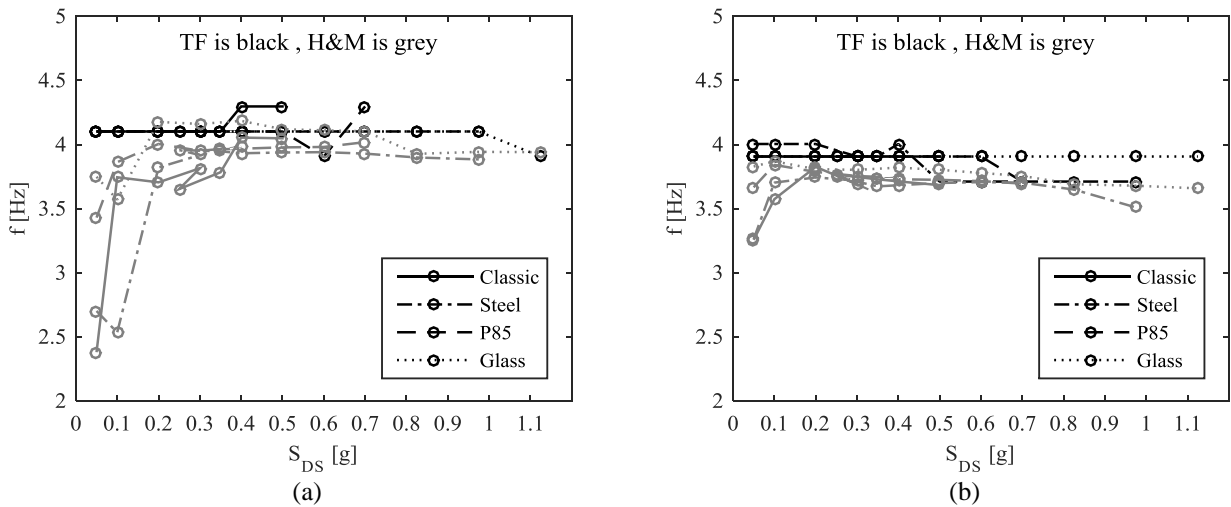
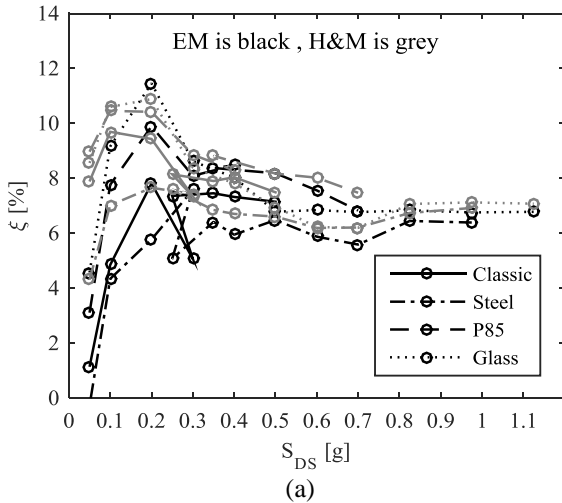
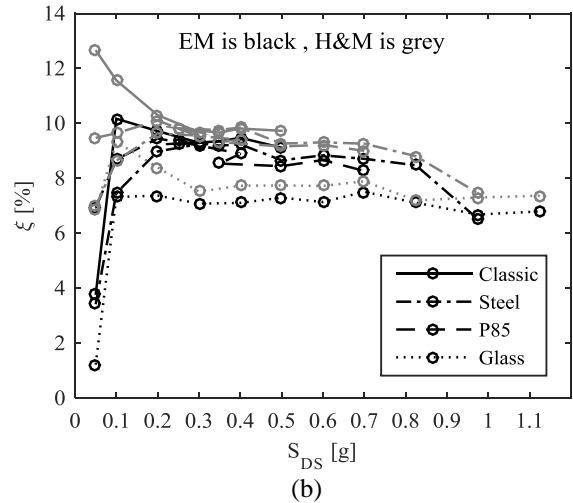


Figure 21. Test frame natural frequency evaluation according to the Transfer Function method (TF, black line) and to the Hashemi and Mosalam (H&M, grey line) procedure for different seismic tests and specimens in (a) X and (b) Y directions



(a)



(b)

505 **Figure 22. Damping ratio evaluation according to the Energetic Method (EM, black line) and to the Hashemi  
506 and Mosalam (H&M, grey line) procedure for different seismic tests and specimens in (a) X and (b) Y directions**

#### 507 4 CONCLUSIONS

508 Shake table tests are performed on temporary internal partitions. A steel frame is designed to exhibit  
509 relative displacements which typically occur at a given story of ordinary buildings. The test frame is  
510 defined in order to subject the partitions to both in-plane interstory drifts and out-of-plane  
511 accelerations. Four different specimens are selected in order to test different panel typologies and  
512 supporting structures: (a) Classic, (b) Steel, (c) P85 and (d) Glass partition systems. The test  
513 campaign also looks at investigating the influence of an innovative device, which was defined  
514 during this test campaign, on the seismic performance of the tested components. The innovative  
515 device aims to avoid the unhooking of the panels from the supporting studs.

516 Several shake table tests are performed subjecting the specimens to interstory drift ratio up to 1.57%  
517 and top acceleration larger than 2.0 g. The hysteretic curves highlight that the partitions do not  
518 contribute to the lateral stiffness of the test setup even for large relative displacements. Recorded  
519 natural frequencies are in the vicinity of the bare natural frequencies in both X and Y direction,  
520 confirming the negligible interaction of the tested specimen with the test frame. The damping ratio  
521 is in the range 5–10%. A significant increase in the damping ratio is exhibited for all the specimens  
522 compared to the bare test setup damping ratio; this increase might be due to the friction developed  
523 by vertical studs, which slide with respect to the horizontal tracks, and by panels hooking system  
524 inside the slotted holes in vertical studs. The amplification factor for out-of-plane acceleration on  
525 walls is in line with the 2.5 amplification factor suggested in ASCE 7 for flexible components.

526 The correlation between the damage state (DS) and the interstory drift ratio (IDR) is performed by  
527 means of a predefined damage scheme. The damage states for standard specimens occur for  
528 interstory drifts in the range 0.41–0.65 for DS1, due to the out-of-plane slight rotation of the panels,  
529 and in the range 0.51–0.81 for DS2, for the fall of a single panel, and DS3, for the fall of more  
530 panels. Fragility curves are also assessed for standard temporary partitions, for applications in  
531 seismic design and other research studies. Significant increase of collapse IDR is recorded with the  
532 introduction of the innovative device, up to IDR larger than 1.44%. It can be therefore concluded  
533 that the simple innovative device significantly improves the seismic performance of the tested  
534 specimens. This study shows that seismic performance of some nonstructural components might be  
535 significantly increased by means of simple modifications aimed at avoiding several failure modes.

#### 536 ACKNOWLEDGEMENTS

537 This study was funded by both the Italian Department of Civil Protection in the frame of the  
538 national project DPC - ReLUIS 2015 task RS8 and Mangini srl, which also provided the partition  
539 systems for the testing program. The contribution of Eng. Luigi Giannetti during the execution of  
540 the tests and Eng. Antonella Guerra, for the results analysis is gratefully acknowledged.

## REFERENCES

- 541  
542 [1] Filiatrault A, Uang CM, Folz B, Christopoulos C, Gatto K. Reconnaissance report of  
543 Nisqually (Seattle-Olympia) February 28, 2001 Earthquake. Report No.SSRP-2001/2002.  
544 Department of Structural Engineering, University of California San Diego. La Jolla, CA.,  
545 2001.
- 546 [2] Dhakal RP. Damage to Non-Structural Components and Contents in the 2010 Darfield  
547 earthquake. *Bulletin of the New Zealand Society for Earthquake Engineering* 2010; **43** (4):  
548 404-411.
- 549 [3] Taghavi S, Miranda E. Response assessment of nonstructural building elements, PEER  
550 report 2003/05. College of Engineering, University of California Berkeley, USA, 2003.
- 551 [4] Earthquake Engineering Research Institute (EERI). Nonstructural Issues of Seismic Design  
552 and Construction, Publication 84-04. Berkeley, CA, USA, 1984.
- 553 [5] Ikuta E, Miyano M. Study of Damage to the Human Body Caused by Earthquakes:  
554 Development of a Mannequin for Thoracic Compression Experiments and Cyber  
555 Mannequin Using the Finite Element Method. In: R. Spence, E. So, C. Scawthorn, editors.  
556 Human Casualties in Earthquakes: Springer Netherlands; 2011. p. 275-289.
- 557 [6] Villaverde R. Seismic design of secondary structures: State of the art. *Journal of Structural  
558 Engineering-Asce* 1997; **123** (8): 1011-1019. DOI:10.1061/(Asce)0733-  
559 9445(1997)123:8(1011).
- 560 [7] Lee TH, Kato M, Matsumiya T, Suita K, Nakashima M. Seismic performance evaluation of  
561 non-structural components: Drywall partitions. *Earthquake Engineering & Structural  
562 Dynamics* 2007; **36** (3): 367-382. DOI:10.1002/eqe.638.
- 563 [8] Restrepo JI, Lang AF. Study of Loading Protocols in Light-Gauge Stud Partition Walls.  
564 *Earthquake Spectra* 2011; **27** (4): 1169-1185. DOI:10.1193/1.3651608.
- 565 [9] Magliulo G, Petrone C, Capozzi V, Maddaloni G, Lopez P, Manfredi G. Seismic  
566 performance evaluation of plasterboard partitions via shake table tests. *Bulletin of  
567 Earthquake Engineering* 2014; **12** (4): 1657-1677. DOI:10.1007/s10518-013-9567-8.
- 568 [10] Cosenza E, Di Sarno L, Maddaloni G, Magliulo G, Petrone C, Prota A. Shake table tests for  
569 the seismic fragility evaluation of hospital rooms. *Earthquake Engineering and Structural  
570 Dynamics* 2014; **44** (1): 23-40. DOI:10.1002/eqe.2456.
- 571 [11] Retamales R, Davies R, Mosqueda G, Filiatrault A. Experimental Seismic Fragility of Cold-  
572 Formed Steel Framed Gypsum Partition Walls. *Journal of Structural Engineering* 2013; **139**  
573 (8): 1285-1293. DOI:10.1061/(ASCE)ST.1943-541X.0000657.
- 574 [12] Soroushian S, Maragakis EM, Jenkins C. Capacity Evaluation of Suspended Ceiling  
575 Components, Part 1: Experimental Studies. *Journal of Earthquake Engineering* 2015; **19**  
576 (5): 784-804. DOI:10.1080/13632469.2014.998354.
- 577 [13] Soroushian S, Maragakis EM, Jenkins C. Capacity Evaluation of Suspended Ceiling  
578 Components, Part 2: Analytical Studies. *Journal of Earthquake Engineering* 2015; **19** (5):  
579 805-821. DOI:10.1080/13632469.2015.1006345.
- 580 [14] Wang DZ, Dai JW. Dynamic Response of Ceiling System with Light Steel Furring and  
581 Gypsum Board under Severe Earthquake. *Applied Mechanics and Materials* 2012; **166-169**  
582 (1): 2221-2225.
- 583 [15] Filiatrault A. Seismic Evaluation of Modular Office Furniture System. *Earthquake Spectra*  
584 1991; **7** (4): 529-541. DOI:10.1193/1.1585641.
- 585 [16] Filiatrault A, Kuan S, Tremblay R. Shake table testing of bookcase – partition wall systems.  
586 *Canadian Journal of Civil Engineering* 2004; **31** (4): 664-676. DOI:10.1139/l04-031.
- 587 [17] Soroushian S, Maragakis EM, Ryan KL, Sato E, Sasaki T, Okazaki T, Mosqueda G. Seismic  
588 Simulation of an Integrated Ceiling-Partition Wall-Piping System at E-Defense. II:  
589 Evaluation of Nonstructural Damage and Fragilities. *Journal of Structural Engineering*  
590 2016; **142** (2): 04015131. DOI:10.1061/(ASCE)ST.1943-541X.0001385.

- 591 [18] Jenkins C, Soroushian S, Rahmanishamsi E, Maragakis EM. Experimental fragility analysis  
592 of cold-formed steel-framed partition wall systems. *Thin-Walled Structures* 2016; **103** 115-  
593 127. DOI:10.1016/j.tws.2016.02.015.
- 594 [19] Petrone C, Magliulo G, Manfredi G. Shake table tests for the seismic assessment of hollow  
595 brick internal partitions. *Engineering Structures* 2014; **72** (0): 203-214.  
596 DOI:10.1016/j.engstruct.2014.04.044.
- 597 [20] American Society of Civil Engineers. ASCE/SEI 7-10: Minimum Design Loads for  
598 Buildings and Other Structures. Reston, Virginia, US, 2010.
- 599 [21] Magliulo G, Pentangelo V, Maddaloni G, Capozzi V, Petrone C, Lopez P, Talamonti R,  
600 Manfredi G. Shake table tests for seismic assessment of suspended continuous ceilings.  
601 *Bulletin of Earthquake Engineering* 2012; **10** (6): 1819-1832. DOI:10.1007/s10518-012-  
602 9383-6.
- 603 [22] Federal Emergency Management Agency (FEMA). Interim protocols for determining  
604 seismic performance characteristics of structural and nonstructural components through  
605 laboratory testing. Report No. FEMA 461. Washington DC, US, 2007.
- 606 [23] CEN. Eurocode 8: design of structures for earthquake resistance - Part 1: general rules,  
607 seismic actions and rules for buildings. EN 1998-1. Brussels, Belgium., 2004.
- 608 [24] Porter K, Kennedy R, Bachman R. Creating Fragility Functions for Performance-Based  
609 Earthquake Engineering. *Earthquake Spectra* 2007; **23** (2): 471-489.  
610 DOI:10.1193/1.2720892.
- 611 [25] Petrone C, Magliulo G, Lopez P, Manfredi G. Seismic fragility evaluation of plasterboard  
612 partitions via in-plane quasi-static tests. *Earthquake Engineering & Structural Dynamics*  
613 2015; **44** (14): 2589-2606. DOI:10.1002/eqe.2600.
- 614 [26] Hashemi A, Mosalam KM. Shake-table experiment on reinforced concrete structure  
615 containing masonry infill wall. *Earthquake Engineering & Structural Dynamics* 2006; **35**  
616 (14): 1827-1852. DOI:10.1002/Eqe.612.
- 617 [27] Chopra AK, *Dynamics of structures: Theory and Applications to Earthquake Engineering*,  
618 Englewood Cliffs, New Jersey, USA, Prentice Hall, 1995.